Simulation of vibrational energy transfer in two-dimensional infrared spectroscopy of amide I and amide II modes in solution

Cite as: J. Chem. Phys. **129**, 055101 (2008); https://doi.org/10.1063/1.2961020
Submitted: 02 April 2008 . Accepted: 27 June 2008 . Published Online: 05 August 2008

Robbert Bloem, Arend G. Dijkstra, Thomas la Cour Jansen, and Jasper Knoester

Simulation of vibrational energy transfer in two-dimensional infrared spectroscopy of amide I and amide II modes in solution

Robbert Bloem, Arend G. Dijkstra, Thomas la Cour Jansen,[a] and Jasper Knoester[b]
Zernike Institute for Advanced Materials, University of Groningen, Nijenborgh 4, 9747 AG Groningen, The Netherlands

(Received 2 April 2008; accepted 27 June 2008; published online 5 August 2008)

Population transfer between vibrational eigenstates is important for many phenomena in chemistry. In solution, this transfer is induced by fluctuations in molecular conformation as well as in the surrounding solvent. We develop a joint electrostatic density functional theory map that allows us to connect the mixing of and thereby the relaxation between the amide I and amide II modes of the peptide building block *N*-methyl acetamide. This map enables us to extract a fluctuating vibrational Hamiltonian from molecular dynamics trajectories. The linear absorption spectrum, population transfer, and two-dimensional infrared spectra are then obtained from this Hamiltonian by numerical integration of the Schrödinger equation. We show that the amide I/amide II cross peaks in two-dimensional infrared spectra in principle allow one to follow the vibrational population transfer between these two modes. Our simulations of *N*-methyl acetamide in heavy water predict an efficient relaxation between the two modes with a time scale of 790 fs. This accounts for most of the relaxation of the amide I band in peptides, which has been observed to take place on a time scale of 450 fs in *N*-methyl acetamide. We therefore conclude that in polypeptides, energy transfer to the amide II mode offers the main relaxation channel for the amide I vibration. © *2008 American Institute of Physics*. [DOI: 10.1063/1.2961020]

I. INTRODUCTION

Energy dissipation plays an important role in many areas of chemistry.[1,2] For example, after a reaction has taken place the excess energy needs to be transported away, possibly to be used to drive a reaction somewhere else. The amide I modes in proteins have been suggested to play an important role in energy transport, for example, following the hydrolysis of adenosine triphosphate.[1] Recent experiments have shown that relaxation from initially excited amide I modes occurs on the picosecond time scale.[3,4] In order to understand dissipation of vibrational energy, studying the ultrafast relaxation processes that play a role in the decay of the amide I mode is important.

N-methyl acetamide (NMA) has been frequently used as a model for the peptide bond,[3–17] which is omnipresent in the backbone of proteins. The amide I mode has been the subject of most studies due to its strong intensity and the strong coupling between different amide I modes, which allow the use of this mode for structural determination.[18–24] Typically the spectra are obtained in heavy water in order to remove the strong water bend signal that is located in the same spectral region as the amide I band. This also results in the exchange of the acidic proton bound to nitrogen, and the resulting molecule is called NMA-d.

Vibrational relaxation from the amide I mode of NMA-d has been investigated both experimentally and theoretically. Experimentally, an overall decay of the amide I vibration with a rate of 450 fs was found[3] using two-dimensional (2D) infrared (IR) spectroscopy. The experimental rate is the sum over all possible decay processes, which include relaxation to the amide II and amide III modes, as well as combinations of lower frequency modes in the protein and the solvent. The relative contributions of these channels to the decay of the amide I mode are still being debated. In a similar molecule (acetylproline-NH_2 in methylene chloride) 36% of the amide I population was found to be transferred to the amide II mode on the same site of the molecule.[25] The transfer took place on a 3.1 ps time scale. A recent 2D IR study used laser pulses broad enough to cover both the amide I and amide II areas of the spectrum and followed the transfer between these two modes more directly.[4] The observed relaxation was on the same time scale as in the previous study. Theoretically, the decay of the amide I mode of NMA-d in D_2O has been the subject of a couple of earlier studies.[26,27] The first was based on classical nonequilibrium simulations with a semiclassical zero-point energy correction.[26] This approach yielded a 1.5 ps relaxation time of the amide I mode but did not report which modes accept the energy, although it should in principle be possible to identify these in the simulation. The second study employed non-Markovian perturbation theory to examine the relaxation from the amide I mode to overtones and combination bands of modes in the frequency range of 550–1130 cm^{-1},[27] thus neglecting relaxation to the amide II mode. An overall vibrational energy relaxation time of 0.5 ps was reported, with the majority of the energy being transferred to a combination of two modes with fundamental frequencies of 612.1 and 1085.8 cm^{-1}. More recently we simulated the transfer between the amide I and amide II modes and calculated the impact on the 2D IR spectrum.[28]

[a]Electronic mail: t.l.c.jansen@rug.nl.
[b]Electronic mail: j.knoester@rug.nl.

The relaxation process was modeled using the Redfield approach with a bath of solvent modes. Information on the effect of the bath was based on the molecular dynamics (MD) simulations and electrostatic mapping that will be presented in the present paper. A population transfer time between the amide I and amide II modes of 560 fs was found.

In our present paper the goal is to simulate the population transfer between the amide I and amide II modes. We will do this by performing numerical integration of the Schrödinger equation (NISE).[29–31] This approach is very general and allows us to account for motional narrowing, rotational dynamics, and non-Condon and non-Gaussian effects, which were not accounted for in our previous study,[28] along with the nonadiabatic effects that lead to population transfer. The only drawback compared to methods that rely on a path integral description of the system-bath interaction[32,33] or on the Redfield approach[28] is that our current treatment assumes the high temperature approximation. In equilibrium all states have equal population instead of the correct thermal population given by the Bose–Einstein distribution, where the amide II mode will have about 60% more population than the amide I mode.[28] Aside from this deficiency, the NISE approach is an excellent approach in its general account of dynamics effects.

Population transfer cannot be measured directly in an experiment. It can, however, be extracted from nonlinear optical experiments such as IR pump/anti-Stokes probe[34] and 2D IR spectroscopy.[3,35–38] In the latter technique an initial pair of laser pulses is used to excite vibrational states. The vibrations are then allowed to evolve freely during a waiting time denoted t_2. Finally the state is probed by applying an additional laser pulse and measuring the emitted signal. Typically the experimental data are analyzed in a 2D contour plot, where for a fixed value of t_2 the frequency of the initially excited states is given along one axis and the frequency of the emitted signal is along the other axis. Information about the interaction between different vibrations can be directly observed through cross peaks.[39,40] One can compare contour plots at different waiting times or plot the signal at individual points in the spectrum as a function of this time to extract information on vibrational dynamics such as vibrational relaxation.[28,41]

The amide I spectra of NMA-d and peptides in solution have been modeled using electrostatic electronic structure maps that were developed for the amide I mode of NMA-d.[7,10,12,14,15,17] This allowed for accurate simulations of the spectra of NMA-d (Refs. 10 and 11) and small peptides.[29,41–48] These maps, however, do not include the coupling with other modes within the NMA-d molecule that is necessary for the description of nonradiative relaxation processes. One study involved four amide modes (I–III and A) but treated them in an adiabatic way, thus discarding the information needed to describe the relaxation between them.[13]

In the present study we will extend the electrostatic map to include both the amide I and II modes of NMA-d, making it possible to calculate the population transfer between those modes. The amide II mode is the most obvious candidate for efficient relaxation from the amide I mode because of the relatively small energy difference between these modes that allows the solvent to easily accept the excess energy. Furthermore, both modes involve the motion of the same carbon atom, suggesting a possible strong interaction between them in solution, which would facilitate efficient energy transfer. The amide I mode is dominated by the CO stretch vibration and the amide II mode is a mixture of CN stretch and CND bend. The normal modes are illustrated in Fig. 1. It has been shown that the amide I mode alone can be modeled accurately with the electrostatic density functional theory (DFT) map.[42] Our assumption is that the same method can be used for the amide II mode. The population transfer will be calculated by constructing a joint electrostatic DFT map for the amide I and amide II modes, which displays how their frequencies, transition dipoles, and mutual coupling depend on the electric field generated by the solvent on the atoms in the peptide unit.

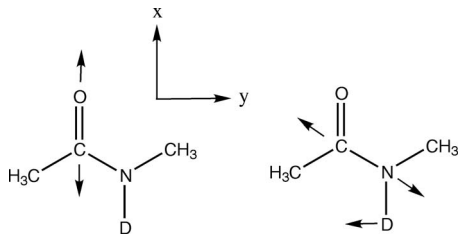

FIG. 1. Left: the amide I vibration. Right: the amide II vibration. The coordinate system used in the simulations and tables is indicated with arrows in the middle.

We will use the developed map to calculate from MD trajectories the Fourier transform IR spectra, population transfer dynamics, and 2D IR spectra with different waiting times. The remainder of this paper is organized as follows. In Sec. II we will describe how the electrostatic DFT map was constructed and we will recapitulate the theory used for the spectral simulations. In Sec. III we will describe results of the MD simulations and the spectral simulations. Finally in Sec. IV we will draw our conclusions.

II. THEORY

A. Electrostatic DFT map construction

The amide I and amide II vibrations of NMA-d in solution will be described with the model Hamiltonian

$$H(t) = \sum_{i=1}^{2} \left[\epsilon_i(t) b_i^\dagger b_i - \frac{\Delta_i}{2} b_i^\dagger b_i^\dagger b_i b_i + \vec{E}(t) \cdot \vec{\mu}_i(t) [b_i + b_i^\dagger] \right] + J_{12}(t)[b_1^\dagger b_2 + b_2^\dagger b_1], \quad (1)$$

where ϵ_i is the harmonic frequency, Δ_i the anharmonicity, and $\vec{\mu}_i$ the transition dipole of the ith gas phase vibrational mode. $b_i^\dagger$ and b_i are the usual bosonic creation and annihilation operators; their index i is 1 for the gas phase amide I mode and 2 for the gas phase amide II mode. The coupling between these two modes is denoted J_{12}. Finally, $\vec{E}(t)$ is the externally applied electric field. In our reduced quantum description, which includes only the amide I and amide II vibrations explicitly, the frequencies, dipoles, and couplings are fluctuating in time due to changes in the surrounding

solvent. These fluctuations of the NMA parameters are assumed to be dominated by changes in the electrostatic field induced by the solvent molecules. This is reasonable as long as the environment mainly consists of polar molecules, such as water and amide units. We can then parametrize the fluctuations in terms of the electric field; this parametrization is obtained using DFT calculations of the molecule in various environments of charges.[10,49,50] The fluctuations of the anharmonicity were found earlier to have little or no effect on the spectra and are therefore neglected in this study.[10] Each fluctuating quantity, generically denoted Ω, is parametrized as a linear combination of the electric field and its gradient generated by the solvent at the positions of the C, O, N, and D atoms of the NMA molecule,

$$\Omega = \Omega_0 + \sum_{a,\alpha} c_{a\alpha} E_\alpha^a, \tag{2}$$

where Ω_0 is the gas phase value, E_α^a is the αth Cartesian component of the electric field or field gradient on atom a, and $c_{a\alpha}$ are the fitting parameters. The summation over α is restricted to the x and y components of the electric field and the zz or xy components of the field gradient (see Fig. 1). The gas phase value Ω_0 and the fitting parameters constitute a transferable electrostatic DFT map. The same procedure was previously applied with success to the amide I mode alone.[10] Here, we extend the method to create a joint map for the amide I frequency ϵ_1, the amide II frequency ϵ_2, and the bilinear coupling constant J_{12}.

Harmonic frequencies were calculated after an initial geometry optimization using DFT. The potential energy surface was obtained by distorting the geometry along the amide I and amide II gas phase modes and calculating the energy. 2D grid on which the potential energy surface was evaluated consisted of 11 points in both dimensions, separated by 0.08 Å. The environment was sampled using the same 75 point charge environments described in Ref. 10. All calculations were performed using the ADF program,[51,52] with the ADF TZ2P basis and the RPBE exchange correlation functional.[53,54] The potential energy surface was expanded in a Taylor series up to the eighth order in both coordinates and the six lowest orders were used to construct a Hamiltonian for the amide I and amide II vibrations.[55] A harmonic basis was used including all basis functions with a total of 21 excitations in the amide I and amide II modes including combination states. The Hamiltonian was diagonalized and the frequencies, coupling, and dipoles were obtained using matrix reconstruction.[17] The map coefficients were then fitted using the electric field and gradients generated by the point charge environments. Fits were performed with both the least-squares method and singular value decomposition. The two methods gave practically identical values for the fit parameters, showing that there are no linear dependencies. In further calculations, we used the fit parameters from the least-squares fit. The correlations between the DFT frequencies and the map frequencies for the 75 fitted point charge configurations were 0.97 and 0.90 for the amide I and amide II site frequencies, respectively. For the coupling the correlation was 0.96. This is slightly lower than the 0.98 correlation found in the earlier study on amide I alone.[10]

TABLE I. The map parameters for the amide I (ϵ_1) and amide II (ϵ_2) frequencies and the coupling between them (J_{12}). The values for Ω_0 are given in cm^{-1}. For the field coefficients the unit is $cm^{-1}/(E_H/e\ \text{bohr})$ and for the gradient coefficients the unit is $cm^{-1}/(E_H/e\ \text{bohr}^2)$. E_H is the Hartree energy unit.

	ϵ_1	ϵ_2	J_{12}
Ω_0	1717.00	1440.00	1.57
c_{Cx}	1947.5	−1112.0	68.5
c_{Cy}	−1415.8	−1645.6	−1408.2
c_{Czz}	−601.9	250.3	−514.6
c_{Cxy}	−6764.5	−3747.6	−6238.7
c_{Ox}	741.0	−319.7	−718.2
c_{Oy}	3097.0	1903.9	3759.4
c_{Ozz}	84.1	−3.6	−169.3
c_{Oxy}	−1923.3	−1471.6	−3332.8
c_{Nx}	641.7	367.8	−88.8
c_{Ny}	313.4	−2896.3	−2756.2
c_{Nzz}	−966.8	−287.4	−506.7
c_{Nxy}	−6776.7	5710.2	3390.8
c_{Dx}	267.3	94.9	100.2
c_{Dy}	−3264.9	4171.1	3072.2
c_{Dzz}	−414.3	48.9	−2.1
c_{Dxy}	−3642.6	3410.3	1595.3

It is known that electronic structure calculations typically predict vibrational frequencies only within 10% of the experimental gas phase values.[56] Because we are interested in the solvent shifts and not in the accuracy of the gas phase predictions, the map was scaled to give the correct gas phase frequencies. For the amide I mode the gas phase frequency is 1717 cm^{-1}. In the case of amide II some discussion exists in the literature due to the presence of two absorption lines in the amide II region.[57,58] These two lines appear at frequencies of 1399 and 1440 cm^{-1} and are most probably caused by a Fermi resonance of the amide II vibration with a combination of low-frequency modes. We used 1440 cm^{-1} as the gas phase amide II frequency.[4,58,59] The difference between the fundamental frequencies obtained by experiment and by our calculation are between 2.5% and 6%, well within the usual margin of accuracy of electronic structure calculations. The anharmonicities were fixed at the experimental values of $\Delta_1 = 16$ cm^{-1} and $\Delta_2 = 11$ cm^{-1}.[4] The transition dipoles for the transitions between the single and double excited states are $\sqrt{2}$ times the transition dipoles from the ground state to the singly excited state, which is a direct consequence of the use of the Hamiltonian in Eq. (1). The final values for the map parameters are listed in Tables I and II. Comparing the amide I coefficients with those reported earlier, quite some differences are observed.[10] This may result from the fact that in the present map the vibration of the methyl groups was included. We also note that the gas phase coupling is not exactly zero, as one might have expected since we use the harmonic gas phase vibrations as our basis set. The reason for this counterintuitive result is that our calculations include anharmonic contributions as well, which introduce a small coupling due to mixing with higher excited harmonic states.

B. Simulation methods

The thus parametrized DFT map relates the Hamiltonian and the transition dipoles to the electrostatic fields and their

TABLE II. The map parameters for the amide I and amide II transition dipoles. The values for Ω_0 are given in D. For the field coefficients the unit is $D/(E_h/e\ \text{bohr})$ and for the gradient coefficients the unit is $D/(E_h/e\ \text{bohr}^2)$. D is the Debye dipole moment unit.

	μ_1^x	μ_1^y	μ_2^x	μ_2^y
Ω_0	0.231	−0.087	0.021	−0.254
c_{Cx}	−0.100	1.361	1.797	−1.009
c_{Cy}	−1.013	4.082	5.430	0.364
c_{Czz}	0.010	0.887	0.399	0.506
c_{Cxy}	−2.606	8.951	11.134	1.602
c_{Ox}	−1.248	0.947	0.412	0.083
c_{Oy}	1.141	−6.815	−8.009	0.305
c_{Ozz}	−0.310	0.146	−0.189	0.517
c_{Oxy}	−0.962	5.358	6.879	−1.097
c_{Nx}	−0.038	−0.944	−1.557	0.358
c_{Ny}	−2.311	1.714	1.376	4.249
c_{Nzz}	−0.230	−0.179	−0.099	0.212
c_{Nxy}	3.946	−1.928	−1.645	−0.438
c_{Dx}	0.035	0.557	0.589	−0.564
c_{Dy}	2.690	−2.943	−2.755	−1.735
c_{Dzz}	−0.486	−0.824	−1.605	1.406
c_{Dxy}	2.133	−1.442	−1.979	−0.951

gradients on the NMA molecule. Time dependence is introduced into the Hamiltonian by the movement of charges in the environment, which in turn leads to a time-varying electric field. Here, we simulated the solvent explicitly using a MD simulation, which gives the positions of molecules in the environment as a function of time. MD simulations were performed using the GROMACS package[60,61] employing the GROMOS87 force field[62–64] for NMA-d and the SPC/E force field for the water molecules. The simulations were performed in the *NPT* ensemble at 300 K and 1 bar.[65,66] We used 346 heavy water molecules and one NMA-d molecule. The simulations were performed for 4 ns, with 1 fs simulation time steps. Snapshots were stored every 10 fs and the DFT map [Eq. (2)] was applied during each snapshot to obtain the Hamiltonian and the transition dipoles. Repeating the procedure for each snapshot, trajectories for the time-dependent Hamiltonian and transition dipoles were obtained.

The resulting fluctuating Hamiltonian [Eq. (1)] was used to calculate the population transfer, as well as the linear absorption spectra and the 2D IR spectra. To calculate these observables, one needs to solve the Schrödinger equation with a time-dependent Hamiltonian,

$$\dot{\phi}(t) = -\frac{i}{\hbar}H(t)\phi(t). \tag{3}$$

During a short time interval Δt, the Hamiltonian is assumed to be constant. The time evolution operator U, which relates the wave function ϕ at time $(n+1)\Delta t$ to the wave function at time $n\Delta t$, is then given by

$$U[(n+1)\Delta t, n\Delta t] = \exp\left[-\frac{i}{\hbar}H_n\Delta t\right]. \tag{4}$$

Here H_n is the fixed Hamiltonian in time interval n. The time evolution over a longer time period can be found by dividing the time in short intervals and multiplying the time evolution operators for each interval. This procedure, called NISE, then gives the time evolution operator $U(\tau_2, \tau_1)$ between two times τ_1 and τ_2.[29]

The linear absorption is determined by the Fourier transform of the two-point correlation function of the transition dipole,

$$I(\omega) = \sum_\alpha \mathrm{Im}\int_0^\infty dt_1 \frac{i}{\hbar}\langle \mu_i^\alpha(\tau_2)U(\tau_2,\tau_1)\mu_i^\alpha(\tau_1)\rangle \times \exp(-i\omega t_1)\Gamma_{LA}(t_1), \tag{5}$$

where $\langle\cdots\rangle$ denotes the ensemble average. Furthermore, τ_2 and τ_1 are the times when the system interacts with the external field and t_1 is the time between these interactions ($t_1 = \tau_2 - \tau_1$). The sum over α is the sum over the three Cartesian components of the dipole vectors. The vibrational lifetime is accounted for by the relaxation factor

$$\Gamma_{LA}(t_1) = \exp(-t_1/2T_1), \tag{6}$$

where T_1 is the lifetime of the singly excited states.

The expressions for the 2D response are given in Eqs. (11)–(14) of Ref. 29. The signal consists of six contributions. These are the ground state bleach, the stimulated emission, and the excited state absorption contributions; all of these come with a rephasing and a nonrephasing part.

The population transfer can be calculated directly from the time evolution operator. The relaxation probability from the amide I to the amide II mode and vice versa is

$$P_{12}(t) = \langle |U_{12}(t,0)|^2\rangle. \tag{7}$$

U_{12} denotes the matrix element between the amide I and amide II gas phase basis states. In the case of incoherent population transfer, starting in a situation where only the amide I mode is excited, $P_{12}(t)$ starts at zero and goes exponentially to the equilibrium value, P_{eq},

$$P_{12}(t) = P_{\text{eq}}[1 - \exp(-t/T_{\text{PT}})]. \tag{8}$$

T_{PT} is the population transfer time. The NISE method implicitly assumes infinite temperature of the solvent, so that $P_{\text{eq}} = 0.5$ and relaxation from amide II to amide I occurs at the same speed as relaxation from amide I to amide II. In the case of coherent transfer, $P_{12}(t)$ will show oscillating behavior at short times.

III. SIMULATION RESULTS

A. Correlation functions

To understand the effect of the environment on the NMA parameters, we calculated the time correlation functions $C(t)$ of the uncoupled amide I and amide II frequencies and the coupling. The correlation function is defined as

$$C(t) = \langle \Omega(t)\Omega'(0)\rangle. \tag{9}$$

The brackets denote the classical ensemble average. Ω and Ω' are the quantities that are correlated. The normalized correlation function is found by dividing with the value of square roots of the autocorrelation functions of these two quantities at time zero. The equal-time correlation constants are shown in Table III, while graphs of the autocorrelation

TABLE III. The correlation constants for the amide vibrations in the gas phase basis.

Ω_1	Ω_2	$\langle\Omega_1(0)\Omega_2(0)\rangle$ (cm^{-2})
ω_I	ω_I	1227.3
ω_{II}	ω_{II}	702.76
J	J	662.72
ω_I	ω_{II}	−499.36
ω_I	J	59.279
ω_{II}	J	489.83

and cross-correlation functions are shown in Figs. 2 and 3, respectively. It is worth noticing that the width of the distribution of the coupling is almost as big as that for the amide II frequency. It is not surprising that two gas phase normal modes are found to be coupled in solution. A constant coupling can in principle be removed by performing a suitable basis transformation. However, solvent induced fluctuations in the coupling cannot be eliminated in this way and lead to relaxation processes. The fact that we find the fluctuations in the coupling to be of considerable magnitude indicates that these fluctuations are important in the description of the relaxation process. As expected from the resonance structure in NMA,[67] the amide I and amide II site frequencies are anticorrelated. The relative correlation coefficient equal to the normalized correlation function at time zero is a measure of the degree of correlation. For the gas phase amide I and amide II frequencies we find a relative correlation coefficient of −0.54, which is large compared to the −0.28 found experimentally on NMA in dimethyl sulfoxide in Ref. 67. Furthermore, the coupling is strongly correlated with the amide II frequency with a relative correlation coefficient of 0.72, while it is practically uncorrelated with the amide I site frequency, where the correlation coefficient is only 0.07. At present, we do not understand the origin of these correlations. We note that correlation between frequency and coupling has been observed experimentally for the amide I and amide A modes.[68] The correlation functions all exhibit a fast initial decay. Recurrences are observed at 250 fs, corresponding to the vibration in the hydrogen bond as discussed in previous studies.[10,28,69] The influence of the hydrogen bond vibration is larger for amide I frequency than that for amide II and it is practically absent in the correlation functions involving the coupling. The transition dipole fluctuations are accounted for. As seen in earlier studies on amide I,[10] the non-Condon effects are small compared to the effects observed in, for example, the OH stretch of water.[70]

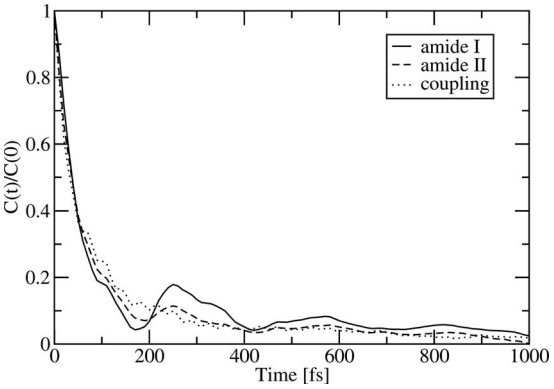

FIG. 2. The normalized autocorrelation functions for the amide vibrations in the gas phase basis, obtained by averaging over 1 (out of 4) ns of the MD simulation.

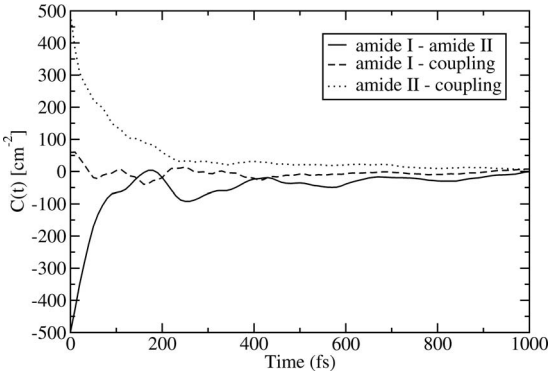

FIG. 3. The cross-correlation functions for the amide vibrations in the gas phase basis, obtained by averaging over 1 (out of 4) ns of the MD simulation.

Our simulation yields a fluctuating Hamiltonian, which is not directly observable experimentally in a bulk sample. In order to assess the quality of the map by making a direct comparison with experiment, we calculated linear IR spectra according to Eq. (5) using a lifetime of 1 ps for both amide modes.[71] The result is shown in Fig. 4 along with the experimental spectrum.[4] Apart from the fact that the simulated spectrum does not include the amide III and IV peaks, the most obvious difference between the simulation and experiment is the observed splitting of the amide II band in the experiment. This double peak structure can be attributed to the presence of a Fermi resonance.[58]

Because the DFT map was scaled to reproduce experimental gas phase results, the frequencies in the solvent can be compared directly to experimental values. The amide I frequency in the solvent is lower than that in the gas phase. Quantitatively, the simulated solvent shift for amide I is −83 cm^{-1}, which compares well to the experimental shift of −94 cm^{-1}. It is similar to the agreement observed in previous studies of the amide I mode.[10,11] For amide II the calculated solvent shift is +21 cm^{-1}, which is smaller than the experimental shift of +53 cm^{-1}.[4] A similar underestimation of the solvent shift was observed in a previous study on

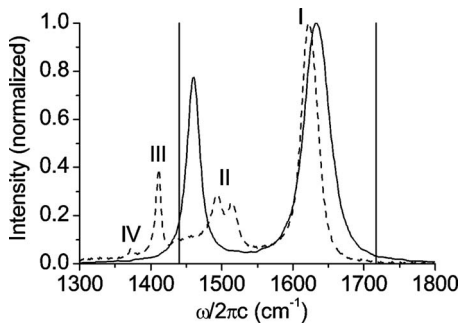

FIG. 4. Experimental (dashed) and simulated (solid) linear spectra. The two vertical lines indicate the gas phase frequencies. The roman numerals label the experimental amide vibrations.

undeuterated NMA (+14 cm^{-1} versus +76 cm^{-1}).[69] This shows that the amide II mode is difficult to model correctly. One reason for this could be the presence of the Fermi resonance; however, in undeuterated NMA this Fermi resonance is not present. Alternatively, the discrepancy could indicate that in contrast to the amide I mode, the amide II mode changes character upon solvation.

To avoid calibration issues we characterize the peaks with the ratio of the intensities between amide I and II. The assignment of intensity to the amide II mode is complicated by the presence of a long tail at the red side of the amide II peak. We make a rough estimate and assign all intensities between the local minima at 1424 and 1554 cm^{-1} to amide II and all intensities above 1554 cm^{-1} to amide I.[28] For the experimental spectrum, the intensity of the amide II peak is then 0.51 of the amide I peak intensity. The same intensity ratio for the calculated spectra is 0.50. In the previous study on undeuterated NMA the experimental ratio was found to be 0.80, as compared to the calculated ratio of 0.66.[69]

B. Linear absorption

The full width at half maximum (FWHM) of the amide I peak is 43 cm^{-1}, compared to the experimental value of 28 cm^{-1} [11] for NMA-d. This comparison is not as good as that observed in the previous studies including only the amide I mode.[10,11] The standard deviation of the amide I frequency in the gas phase basis is only 35 cm^{-1}. This indicates that the coupling with the amide II mode results in additional line broadening. The FWHM of the calculated amide II peak is 22.4 cm^{-1}, which is similar to the standard deviation of 26.5 cm^{-1} of the amide II frequency in the gas phase basis. The FWHM cannot be compared to an experimental value due to the presence of the Fermi resonance.

C. Two-dimensional spectra and population transfer

In the case of NMA, the widths of linear absorption lines are dominated by frequency fluctuations, implying that direct information about population relaxation is difficult to extract. It is, however, possible to extract such information from the 2D IR experiment. A selection of simulated absorptive 2D IR spectra is shown in Fig. 5 for the magic angle polarization. This polarization is also often called the isotropic or rotation-free signal since rotational effects are eliminated. This polarization is obtained by keeping an angle of 54.7° between the pump and probe pulses.[72] Again, the Fermi resonance is not observed and the simulated amide II peak is located at a too low frequency, as already observed for the linear spectrum. In addition to these features, it is clear that the four peak pairs look quite different. The amide I diagonal peak is somewhat stretched along the diagonal at short waiting times while losing its tilt at longer times. This indicates spectral diffusion from an initial inhomogeneous distribution of frequencies. The amide II diagonal peak exhibits little spectral evolution, indicating that the amide II mode is in the homogeneous line broadening regime. Even though the fluctuations in the amide II frequency are significant, their time scale ($1/\Lambda=91$ fs) is fast enough to make the line appear homogeneous. This can be seen quantitatively from the line

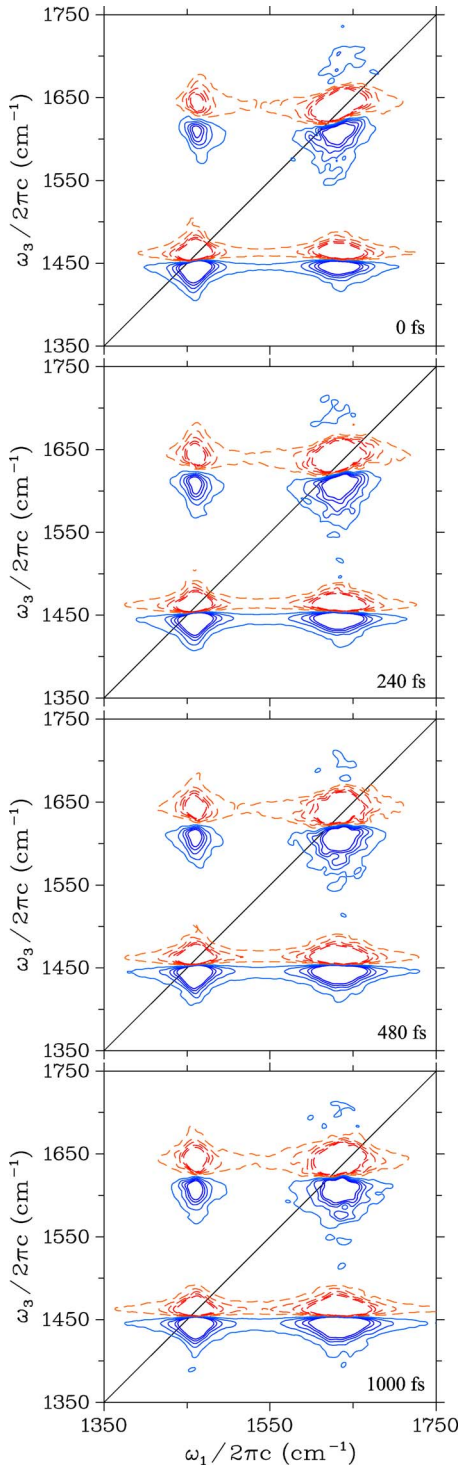

FIG. 5. (Color online) The simulated 2D IR spectrum is shown for different waiting times. The spectra are shown for the magic angle polarization. The intensity is shown in ten steps between ± 0.04, ± 0.08, ..., ± 0.20. Blue (solid) contours encode induced absorption peaks; bleaching and stimulated emission processes are shown as red (dashed) contours. Each spectrum is normalized to the maximum intensity.

broadening parameter κ,[73] which has a value of 2.7 for the amide II mode. This is almost twice the value of $\kappa=1.4$ found for the amide I mode, where the fluctuations are larger and slightly slower ($1/\Lambda=117$ fs). The upper cross peak is somewhat stretched along the ω_3 axis since the amide I frequencies have a broader distribution than the amide II fre-

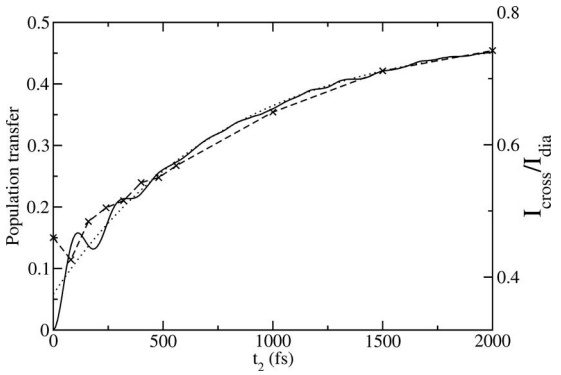

FIG. 6. The calculated population transfer (solid line) is shown along with the relative cross peak intensity (dashed line, crosses indicate data points) extracted from the simulated 2D IR spectra with magic angle polarization and the exponential fit to the population transfer (dotted line).

quencies. For the same reason the lower cross peak is stretched along the ω_1 axis. Both cross peaks exhibit a slight antidiagonal tilt, which is a signature of anticorrelation between the amide I and amide II frequencies.[74] This tilt is more obvious in the upper cross peak than in the lower one because the latter is stretched along the ω_1 axis, thereby decreasing the tilting angle. The antidiagonal tilt is in good agreement with the calculated correlation coefficient between the frequencies in the gas phase basis. The presence of coupling can be expected to result in additional anticorrelation. Due to fast spectral diffusion the observed tilt disappears as the waiting time increases. The cross peak tilt effect was already observed experimentally for NMA in DMSO.[67]

The population transfer can be connected to the 2D IR spectra. The ground state bleach contribution is not affected by population transfer during the waiting time, while both the stimulated emission and excited state absorption parts are. Population transfer leads to a growth in the cross peaks between the involved states and a decrease in the diagonal peaks. Memory effects, rotational motion, and lifetime decay also lead to changes in the spectrum as the waiting time t_2 is changed. This complicates the extraction of population transfer rates from the experimental spectra. In simulation, the population transfer between the gas phase basis functions is readily calculated from Eq. (7). The calculated population transfer is shown in Fig. 6 along with the relative cross peak intensity. The relative cross peak intensity was calculated by integrating the intensity under the subdiagonal cross peaks and dividing by the integrated intensity under the diagonal amide I peak. The integrals were performed in the square frequency intervals defined by the frequency ranges of 1450–1475 cm^{-1} for the amide II and 1625–1675 cm^{-1} for amide I. The directly calculated population transfer was fitted to Eq. (8). A decay time of 790 fs is found. Comparing the calculated transfer with the relative cross peak intensity shows that the latter gives a good measure of the population transfer at long times. At short times, dynamic effects, such as spectral diffusion and coherent contributions, contaminate the spectra. The calculated population transfer shows a slight trace of oscillations, indicating a weak initial coherent transfer. However, the transfer can be well described as incoherent.

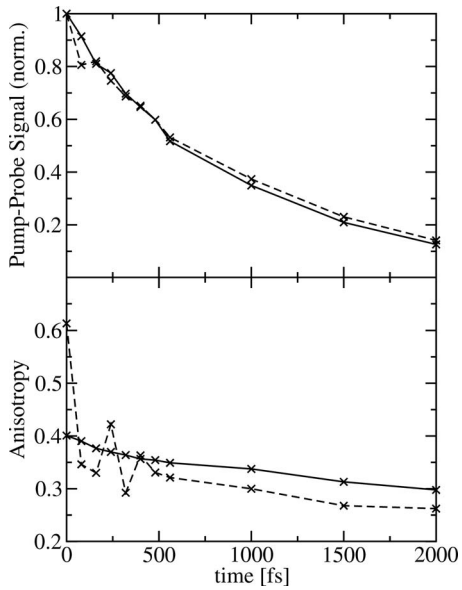

FIG. 7. Upper panel: The calculated pump-probe signal with a broad pump and narrow probe in the amide I (solid line) and amide II (dashed line) regions. Lower panel: The calculated polarization anisotropy for the diagonal amide I (full line) and amide II (dashed line) regions. The crosses indicate data points.

The total decay rate is the sum of the decay rates of individual processes. Experimental work shows the overall lifetime of amide I to be 450 fs.[3] Using the fact that the sum of the rates of all processes adds up to the total decay rate, the shortest decay time of a single competing process cannot be faster than 1045 fs when one identifies the total decay with the experimentally observed value. This means that the population transfer to the amide II mode accounts for more than half of the decay process of the amide I mode. Our finding contradicts earlier calculations that suggested that the amide I decay process is dominated by a subpicosecond relaxation to a set of low-frequency modes.[27,75] They do, however, support our earlier findings using the Redfield approach.[28]

One of the important factors that influences the population transfer time found in our calculation is the energy gap between the amide I and amide II modes. The underestimation of the solvent shift results in a calculated gap that is larger than the experimental result. A smaller gap usually enhances the transfer rate. In our previous study,[28] we used the fluctuations from the map found in the present paper but fixed the frequency difference between the amide I and amide II modes at the experimental value. This approach gave a population transfer time of only 560 fs,[28] indicating that the amide II mode is the prime relaxation pathway for the amide I mode. We would therefore expect the decay rate to increase in a comparable manner if the solvent shift of the amide II mode were better described by our electrostatic map.

We extracted the broad pump narrow probe signal from the 2D spectra. This was done by integrating the magic angle polarization signal over all ω_1 and the frequency ranges 1450–1475 cm^{-1} for amide II and 1625–1675 cm^{-1} for amide I along the ω_3 axis. The result is shown in Fig. 7 (upper panel), where similar decays are seen for the two

regions. This is in contrast to the experimental observations of Ref. 4. This result is not unexpected, since we assumed the same decay rate from the amide I and amide II states back to the ground state. Furthermore, the NISE method yields a high temperature approximation and in equilibrium all states will have identical population independent of their energy. In order to catch the experimentally observed differences, one will need to perform simulations in a density matrix framework[28,73] instead of the wave function framework employed here. In the experimental pump-probe signal[4] a distinctive beat is observed when the amide II frequency is probed. This beat is peaking at 250 fs. In the simulated pump-probe spectra there is a hint of such feature, but it is much weaker than that in the experiment.

Polarization anisotropy is sensitive to rotation and in the simple case of one vibration, it equals the rotational correlation function. We calculated the anisotropy for the diagonal peaks integrating the signal over the same frequency regions already discussed using the expression

$$r(t) = \frac{S_{\parallel}(t) - S_{\perp}(t)}{S_{\parallel}(t) + 2S_{\perp}(t)}. \tag{10}$$

Here $r(t)$ is the anisotropy and $S_{\parallel}(t)$ and $S_{\perp}(t)$ are the signals obtained using laser fields polarized parallel to each other and perpendicular pump and probe laser fields, respectively. The calculated anisotropy is shown in Fig. 7 (lower panel). A significant difference is observed between the amide I and amide II modes. While the anisotropy of the amide I mode decays monotonically, the anisotropy of the amide II mode shows a damped oscillation with the first beat at 250 fs.

A further analysis of the amide II normal mode shows that the hydrogen atoms in the methyl groups move quite a lot. Furthermore, quite a few modes involving motion of these hydrogen atoms have an energy close to that of the amide II mode. These modes were neglected in both our parametrization of the amide II mode of NMA-d and in that of others observing the same problem with describing the amide II mode in NMA.[69] These modes might be involved in the observed Fermi resonance as well. This indicates that the problem with the underestimated solvent shift could be connected to the mixing with these modes. This problem can be circumvented in two ways. One could include all the modes in the vicinity of the amide II mode in the parametrization, which would be very time consuming both when constructing the map and when simulating the spectra. Alternatively one could construct an electrostatic map for the NMA$-d_7$ isotopomer, where the hydrogen vibrations have been moved down considerably in frequency, efficiently separating them from the amide II mode. Such a map could probably be used for calculating spectra of real proteins as well, since most of the hydrogen atoms are replaced here by amino acid side groups and protein backbone atoms. Constructing such a map is work in progress.

IV. CONCLUSION

We constructed an electrostatic map for the amide I and amide II vibrations that allows us to extract the fluctuating vibrational Hamiltonian from the electric field exerted on the NMA-d molecule by solvent molecules. We parametrized the site frequencies, the coupling, and the transition dipoles in terms of local electrical fields and electrical field gradients. We combined the electrostatic map with MD simulations on NMA-d in heavy water to calculate the population transfer, linear absorption, and 2D IR spectra using numerical integration of the Schrödinger equation. In this way we included dynamic effects, such as molecular rotation, vibrational population transfer, non-Gaussian frequency fluctuations, coupling fluctuations, and non-Condon effects in our model.

For amide I we found a solvent shift comparable to earlier studies and in good agreement with experiment. The shift for amide II was much smaller than that experimentally observed. The same problem was observed in previous simulations in NMA.[69] The amide II mode is further observed to give rise to a Fermi resonance in the experiment, a feature that we have not included in our simulations. In our DFT calculations we found several normal modes involving hydrogen vibrations on the methyl groups in the same frequency range as the amide II mode. The underestimation of the amide II solvent shift and the Fermi resonance can arise from mixing with these modes. We are presently constructing an electrostatic map for NMA$-d_7$ to see if eliminating the methyl hydrogens improves the accuracy.

We calculated a population transfer time from amide I to amide II of 790 fs, which is slower than the experimentally observed amide I lifetime of 450 fs decay. The slower decay can be explained either by decay to other modes than amide II or by the simple fact that in the present calculations the energy gap between the amide I and amide II modes is underestimated. In our previous Redfield approach, using the same fluctuating Hamiltonian found in the present study but correcting the gap to reproduce its experimental value, a population transfer time of 560 fs was reported.[28] Both findings, however, suggest that the population transfer from amide I to amide II is the predominant relaxation pathway for the amide I mode.

We compared the directly simulated population transfer with the one extracted from simulated 2D IR spectra. The intensity ratio between the cross peak and the diagonal peak gives a good measure for the population transfer at longer times, while at short times effects from coherent contributions and possibly spectral diffusion affect the intensity ratio. The decay of the pump-probe spectra was practically identical for amide I and amide II. This is in contrast to experimental observations. In the present approach all populations are assumed to decay to the ground state with the same rate. In reality this is unlikely to be the case. The amide I mode is likely to decay through the amide II mode, which decays further to the ground state possibly through one or more intermediate modes. Simulations in the density matrix framework are needed in order to treat such effects.

While there is room for improvement, the present results show that we can simulate population transfer and vibrational spectra including spectral diffusion and molecular rotation, obtaining reasonably good agreement with experiment. The method proposed here will allow to obtain valuable information on the population transfer observed in peptides and possibly small proteins.

ACKNOWLEDGMENTS

T.l.C.J. acknowledges the Netherlands Organization for Scientific Research (NWO) for support through a VENI grant. Andrei Tokmakoff and Lauren DeFlores are gratefully acknowledged for providing their experimental data. The authors thank Ria Broer for helpful discussions.

[1] A. S. Davydov, *Solitons in Molecular Systems* (Reidel, Dordrecht, 1985).
[2] A. Laubereau and W. Kaiser, Rev. Mod. Phys. **50**, 607 (1978).
[3] P. Hamm, M. H. Lim, and R. M. Hochstrasser, J. Phys. Chem. B **102**, 6123 (1998).
[4] L. DeFlores, Z. Ganim, S. F. Ackley, H. S. Chung, and A. Tokmakoff, J. Phys. Chem. B **110**, 18973 (2006).
[5] S. Krimm and J. Bandekar, Adv. Protein Chem. **38**, 181 (1986).
[6] N. G. Mirkin and S. Krimm, J. Mol. Struct. **377**, 219 (1996).
[7] P. Bour, D. Michalik, and J. Kapitan, J. Chem. Phys. **122**, 144501 (2005).
[8] H. Torii, J. Phys. Chem. A **108**, 7272 (2004).
[9] H. Torii and M. Tasumi, J. Chem. Phys. **96**, 3379 (1992).
[10] T. l. C. Jansen and J. Knoester, J. Chem. Phys. **124**, 044502 (2006).
[11] M. F. DeCamp, L. DeFlores, J. M. McCracken, A. Tokmakoff, K. Kwac, and M. Cho, J. Phys. Chem. B **109**, 11016 (2005).
[12] J. R. Schmidt, S. A. Corcelli, and J. L. Skinner, J. Chem. Phys. **121**, 8887 (2004).
[13] W. Zhuang, D. Abramavicius, T. Hayashi, and S. Mukamel, J. Phys. Chem. B **110**, 3362 (2006).
[14] S. Ham and M. Cho, J. Chem. Phys. **118**, 6915 (2003).
[15] K. Kwac and M. H. Cho, J. Chem. Phys. **119**, 2247 (2003).
[16] P. Bour and T. A. Keiderling, J. Chem. Phys. **119**, 11253 (2003).
[17] J. H. Choi, S. Y. Ham, and M. Cho, J. Phys. Chem. B **107**, 9132 (2003).
[18] N. Demirdöven, C. M. Cheatum, H. S. Chung, M. Khalil, J. Knoester, and A. Tokmakoff, J. Am. Chem. Soc. **126**, 7981 (2004).
[19] A. Barth, Biochim. Biophys. Acta **1767**, 1073 (2007).
[20] S. Woutersen and P. Hamm, J. Chem. Phys. **115**, 7737 (2001).
[21] H. Maekawa, C. Toniolo, Q. B. Broxterman, and N. H. Ge, J. Phys. Chem. B **111**, 3222 (2007).
[22] A. G. Dijkstra and J. Knoester, J. Phys. Chem. B **109**, 9787 (2005).
[23] S. Woutersen and P. Hamm, J. Chem. Phys. **114**, 2727 (2001).
[24] R. Schweitzer-Stenner, F. Eker, Q. Huang, and K. Griebenow, J. Am. Chem. Soc. **123**, 9628 (2001).
[25] I. V. Rubtsov and R. M. Hochstrasser, J. Phys. Chem. B **106**, 9165 (2002).
[26] P. H. Nguyen and G. Stock, J. Chem. Phys. **119**, 11350 (2003).
[27] H. Fujisaki, Y. Zhang, and J. E. Straub, J. Chem. Phys. **124**, 144910 (2006).
[28] A. G. Dijkstra, T. l. C. Jansen, R. Bloem, and J. Knoester, J. Chem. Phys. **127**, 194505 (2007).
[29] T. l C. Jansen and J. Knoester, J. Phys. Chem. B **110**, 22910 (2006).
[30] T. l C. Jansen, W. Zhuang, and S. Mukamel, J. Chem. Phys. **121**, 10577 (2004).
[31] H. Torii, J. Phys. Chem. A **110**, 4822 (2006).
[32] A. Ishizaki and Y. Tanimura, J. Phys. Chem. A **111**, 9269 (2007).
[33] A. Ishizaki and Y. Tanimura, J. Chem. Phys. **125**, 084501 (2006).
[34] J. C. Deak, S. T. Rhea, L. K. Iwaki, and D. D. Dlott, J. Phys. Chem. A **104**, 4866 (2000).
[35] S. Mukamel, Annu. Rev. Phys. Chem. **51**, 691 (2000).
[36] D. M. Jonas, Annu. Rev. Phys. Chem. **54**, 425 (2003).
[37] J. C. Wright, Int. Rev. Phys. Chem. **21**, 185 (2002).
[38] R. M. Hochstrasser, Proc. Natl. Acad. Sci. U.S.A. **104**, 14190 (2007).
[39] O. Golonzka, M. Khalil, N. Demirdöven, and A. Tokmakoff, J. Chem. Phys. **115**, 10814 (2001).
[40] M. Khalil and A. Tokmakoff, Chem. Phys. **266**, 213 (2001).
[41] T. l C. Jansen and J. Knoester, Biophys. J. **94**, 1818 (2008).
[42] T. l C. Jansen, A. G. Dijkstra, T. M. Watson, J. D. Hirst, and J. Knoester, J. Chem. Phys. **125**, 044312 (2006).
[43] H. Torii, J. Phys. Chem. B **111**, 5434 (2007).
[44] Z. Ganim and A. Tokmakoff, Biophys. J. **91**, 2636 (2006).
[45] R. D. Gorbunov, P. H. Nguyen, M. Kobus, and G. Stock, J. Chem. Phys. **126**, 054509 (2007).
[46] R. D. Gorbunov and G. Stock, Chem. Phys. Lett. **437**, 272 (2007).
[47] S. Ham, S. Hahn, C. Lee, T.-K. Kim, K. Kwac, and M. Cho, J. Phys. Chem. B **108**, 9333 (2004).
[48] S. Hahn, S. Ham, and M. Cho, J. Phys. Chem. B **109**, 11789 (2005).
[49] C. J. Fecko, J. D. Eaves, J. J. Loparo, A. Tokmakoff, and P. L. Geissler, Science **301**, 1698 (2003).
[50] S. A. Corcelli, C. P. Lawrence, and J. L. Skinner, J. Chem. Phys. **120**, 8107 (2004).
[51] G. te Velde, F. M. Bickelhaupt, E. J. Baerends, C. Fonseca Guerra, S. J. A. v. Gisbergen, J. G. Snijders, and T. Ziegler, J. Comput. Chem. **22**, 931 (2001).
[52] C. F. Guerra, O. Visser, J. G. Snijders, G. te Velde, and E. J. Baerends, in *Methods and Techniques in Computational Chemistry, METECC-5*, edited by E. Clementi and G. Corongiu (STEF, Cagliari, Italy, 1995).
[53] J. P. Perdew, K. Burke, and M. Ernzerhof, Phys. Rev. Lett. **77**, 3865 (1996).
[54] B. Hammer, L. B. Hansen, and J. K. Norskov, Phys. Rev. B **59**, 7413 (1999).
[55] J. Dreyer, J. Chem. Phys. **122**, 184306 (2005).
[56] F. Jensen, *Introduction to Computational Chemistry* (Wiley, Chicester, UK, 1999).
[57] A. A. Balazs, J. Mol. Struct. **153**, 103 (1987).
[58] L. C. Mayne and B. Hudson, J. Phys. Chem. **95**, 2962 (1991).
[59] X. G. Chen, R. Schweitzer-Stenner, S. A. Asher, N. G. Mirkin, and S. Krimm, J. Phys. Chem. **99**, 3074 (1995).
[60] E. Lindahl, B. Hess, and D. v. d. Spoel, J. Mol. Model. **7**, 306 (2001).
[61] H. J. C. Berendsen, D. van der Spoel, and R. van Drunen, Comput. Phys. Commun. **91**, 43 (1995).
[62] W. F. van Gunsteren and H. J. C. Berendsen, Mol. Phys. **34**, 1311 (1977).
[63] A. R. van Buuren, S. J. Marrink, and H. J. C. Berendsen, J. Phys. Chem. **97**, 9206 (1993).
[64] A. E. Mark, S. P. van Helden, P. E. Janssen, and W. F. van Gunsteren, J. Am. Chem. Soc. **116**, 6293 (1994).
[65] H. J. C. Berendsen, J. P. M. Postma, W. F. v. Gunsteren, A. DiNola, and J. R. Haak, J. Chem. Phys. **81**, 3684 (1984).
[66] M. P. Allen and D. J. Tildesley, *Computer Simulation of Liquids* (Oxford University Press, Oxford, 1987).
[67] I. V. Rubtsov, J. Wang, and R. M. Hochstrasser, Proc. Natl. Acad. Sci. U.S.A. **100**, 5601 (2003).
[68] I. V. Rubtsov, J. Wang, and R. M. Hochstrasser, J. Chem. Phys. **118**, 7733 (2003).
[69] T. Hayashi, W. Zhuang, and S. Mukamel, J. Phys. Chem. A **109**, 9747 (2005).
[70] J. R. Schmidt, S. A. Corcelli, and J. L. Skinner, J. Chem. Phys. **123**, 044513 (2005).
[71] Reference 11 shows that the likely lifetime for this system is between 1000 and 2000 ps. Calculations with several lifetimes between 700 and 10 000 fs showed negligible differences between the linear spectra.
[72] R. M. Hochstrasser, Chem. Phys. **266**, 273 (2001).
[73] S. Mukamel, *Principles of Nonlinear Optical Spectroscopy* (Oxford University Press, New York, 1995).
[74] R. Venkatramani and S. Mukamel, J. Chem. Phys. **117**, 11089 (2002).
[75] H. Fujisaki, K. Yagi, K. Hirao, and J. E. Straub, Chem. Phys. Lett. **443**, 6 (2007).